RSC Advances

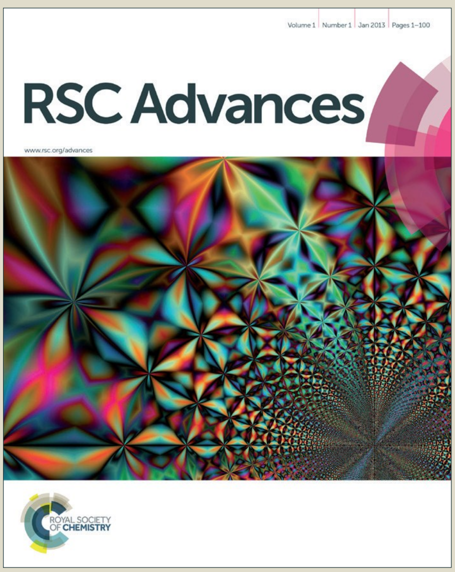

RSC Advances

PAPER

Received 00th January 20xx,
Accepted 00th January 20xx

DOI: 10.1039/x0xx00000x

www.rsc.org/

A F-ion Assisted Preparation Route to Improve the Photodegradation Performance of TiO_2@rGO System-How to Efficiently Utilize the Photogenerated Electrons in the Target Organic Pollutants

Linjuan Guo,[a,b‡] Zheng Yang,[a, b‡] Baiyi Zu,[a] Bin Lu[a] and Xincun Dou*[a]

The comparison of the work function of reduced graphene oxide (rGO) and the conduction band position of TiO_2 reveals that the density of TiO_2 particles grown on rGO could affect the photodegradation efficiency of a TiO_2@rGO heterojunction. Herein, with the introduction of F-ion into the preparation route, F-doped shaped TiO_2 nanocrystals are densely and uniformly decorated on rGO sheets *via* the ice bath hydrolyzation method. Thus, more dye molecules are adsorbed on the surface of TiO_2 and the photogenerated electrons in the excited dye molecules could be efficiently utilized to improve the overall photodegradation efficiency. The as-prepared F-doped TiO_2@rGO heterojunction showed extremely high photocatalytic efficiency under UV-vis light irradiation compared with that of the commercial P25 and the mixture of F-TiO_2 and rGO. It is proved that the ice bath hydrolyzation preparation route is crucial to improve the photodegradation efficiency of the final product since the pure TiO_2@rGO heterojunction is also much more efficient than the mixture of F-TiO_2 and rGO. The present work provides new insights into efficiently utilizing the photogenerated electrons in the target organic pollutants.

1. Introduction

Photodegradation of organic pollutants has attracted extensive attention during the past decades due to its great potential in confronting energy and environmental challenges.[1-7] TiO_2 is regarded as one of the most promising candidate materials in the field of photocatalysis for its low toxicity, strong ultraviolet (UV) light absorption, excellent chemical and thermal stability and resistance to photocorrosion.[8-10] Up to now, a series of TiO_2 and TiO_2-based materials have been widely applied in the photodegradation and detection of pollutants in air or water.[11-15] Especially, the composites of TiO_2 and carbon (TiO_2-C) are currently being considered as potential photocatalysts in the purification of air and water.[2, 16-25]

RGO, owing to the large specific surface area, excellent conductivity, mechanical and chemical stability, [26] has received considerable attention in many potential applications.[27-35] Moreover, the functional groups of rGO could provide reactive sites for surface chemical modification, which facilitates its use in composites materials.[2, 36, 37] Therefore, the combination of TiO_2 and rGO (TiO_2@rGO) could be much more promising to improve the photocatalytic performance of TiO_2 due to the vectorial transfer of photogenerated electrons from TiO_2 to rGO sheets which effectively suppresses the charge recombination, leaving more hole carriers and promoting the degradation of dyes.[38-41] Up to now, there are many reports on the photocatalytic application of the TiO_2@rGO-based materials.[42-44] Though the photocatalytic activity has been greatly enhanced compared with pure TiO_2, the photodegradation is generally realized by utilizing the photogenerated electron-hole pairs in TiO_2. Thus, the importance of efficient utilization of the photogenerated electrons in the target degradation dye molecules is always ignored. It is known that the work function of rGO (-4.42 eV) is larger than the conduction band position of TiO_2 (-4.40 eV), and the injection rate of the electrons from the excited dyes* into the rGO sheets is even faster than that into TiO_2.[44, 45] However, the injected electrons in rGO could hardly promote the subsequent degradation efficiency.[44, 45] Only those excited dyes adsorbed on the surface of TiO_2 could directly inject electrons into TiO_2, forming reactive oxygen species (ROSs) on TiO_2. The dyes which lost electrons are subsequently degraded by these ROSs, thus greatly enhancing the degradation efficiency. Rhodamine B (RhB) is a typical simulating organic pollutant molecule frequently used for evaluating the photodegradation efficiency of a photocatalyst. The work function of RhB and excited RhB* are -5.45 and -3.08 eV, respectively.[44, 45] When RhB is used to evaluate the

[a.] Laboratory of Environmental Science and Technology, Xinjiang Technical Institute of Physics & Chemistry; Key Laboratory of Functional Materials and Devices for Special Environments, Chinese Academy of Sciences, Urumqi 830011, China. xcdou@ms.xjb.ac.cn
[b.] University of Chinese Academy of Sciences, Beijing 100049, China.
† Electronic Supplementary Information (ESI) available: XPS, SEM, UV-vis absorption spectrum, and the size distribution. See DOI: 10.1039/x0xx00000x

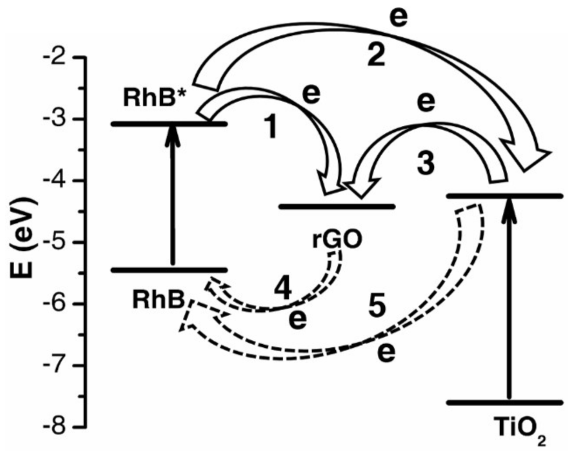

Scheme 1. The energy band diagram of RhB and a TiO_2@rGO system (Lines 1, 2 and 3 stand for the transfering route of the photogenerated electrons in RhB*; lines 4 and 5 stand for the recombination process of the electrons with $RhB^{\bullet+}$).

photodegradation efficiency of a TiO_2@rGO system, the energy band diagram can be expressed by Scheme 1. It is shown that if the surface of rGO sheets is not fully covered with TiO_2 nanoparticles, most of the RhB molecules will be adsorbed on rGO, the photogenerated electrons in the excited RhB* cannot flow to TiO_2 (line 1 in Scheme 1) and have little contribution to the photocatalytic activity. On the contrary, if most of the RhB molecules are adsorbed on TiO_2 nanoparticles, the excited RhB* could directly inject electrons into TiO_2 (line 2 in Scheme 1), thus the photogenerated electrons in RhB* could be efficiently utilized. Therefore, the dense and uniform growth of TiO_2 on rGO sheets, which is beneficial for the adsorption of the majority of dyes on the surface of TiO_2, is crucial to improve the photodegradation efficiency of the TiO_2@rGO system. However, this critical issue has been ignored for a long time and the realization and control of dense and uniform growth of TiO_2 on rGO sheet is still a great challenge.[46]

Herein, the ice bath hydrolyzation method is adopted to achieve the dense and uniform growth of anatase TiO_2 nanoparticles on rGO sheets. Furthermore, F-ions are introduced to further improve the crystallinity of TiO_2 nanoparticles. The F-doped TiO_2@rGO can completely photodegrade the RhB solution with a concentration of 30 mg/L within 6 min under UV-vis light irradiation, which is in sharp contrast with the F-doped TiO_2-rGO mixture, which can only degrade 60% of the RhB. It is proved that the dense cover of TiO_2 nanoparticles on rGO sheets, no matter with or without the doping of F-ion, can help to efficiently utilize the photogenerated electrons in the target RhB molecules to enhance the final photodegradation efficiency.

2. Experimental

2.1. Catalyst Preparation

Graphene oxide (GO) was prepared using a modified Hummers' method.[47, 48] 0.55 mL of $TiCl_4$ kept in a refrigerator was extracted using a 1 mL syringe and rapidly injected into the bottom of a parafilm sealed 100 mL bottle with 50 mL of Deionized (DI) water in the form of ice. After that, the bottle was firmly covered with the bottle cap and shaken continuously until the ice was dissolved. In the whole process, no white precipitation was observed. Then 9.57 mL of GO solution (4.6 mg/mL) was injected into the above bottle under stirring to disperse it well. After that, 0.21 g of NaF was added to the above TiO_2/GO solution to prepare the F-doped rGO@TiO_2 heterojunction. Then the solution was kept stirring in a water bath at 50 °C for 48 h. The color of the solution turned from transparent to gray slowly. The precipitate was collected by centrifugation after being washed with DI water and ethanol several times and then was dried completely at 70 °C. Finally, the product was kept in a ceramic crucible and annealed in a tubular oven at 500 °C for 120 min with nitrogen gas protection. For the preparation of pure TiO_2@rGO heterojunction: all the procedures were the same with that of F-doped TiO_2@rGO heterojunction without the addition of NaF in the precursor solution. The weight ratio of rGO in these two samples is 11%. The other TiO_2@rGO heterojunctions with different weight ratios of rGO were obtained by tuning the volume of the GO solution.

2.2. Catalyst Characterization

X-ray diffraction (XRD) measurement was carried out using powder XRD (Bruker D8 Advance, with Cu K_α radiation operating at 40 kV and 40 mA, scanning from 2θ = 10° to 80°). Transmission electron microscope (JEM-2011 TEM, 200 kV) and Raman spectroscopy (LabRAM HR Evolution, 532 nm) were used to characterize the samples. The X-ray photoelectron spectroscopy (XPS) measurement was conducted on a EscaLab 250Xi spectrometer (Thermo Scientific) using monochromatic Al K_α X-ray source (anode HT = 15 kV) operating at a vacuum higher than $2*10^{-9}$ mbar. Nitrogen adsorption-desorption isotherms were measured on the system (Quantachrome, USA) at -196 ^{o}C. The specific surface area and porosity property analysis was calculated by the Braunauer-Emmett-Teller (BET) method. The optical property of the present nanocomposites was measured with diffuse reflectance UV-vis spectrometer (Shimadzu, SolidSpec-

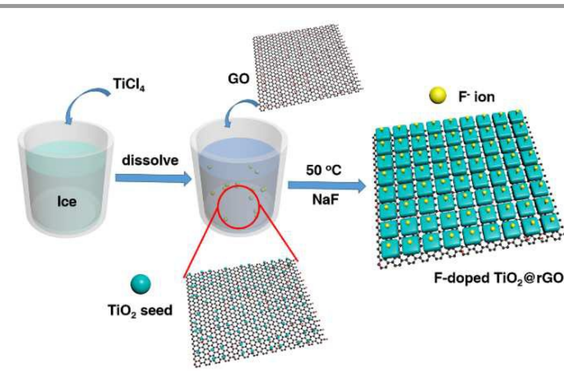

Scheme 2. The preparation route of the F-doped TiO_2@rGO heterojunction.

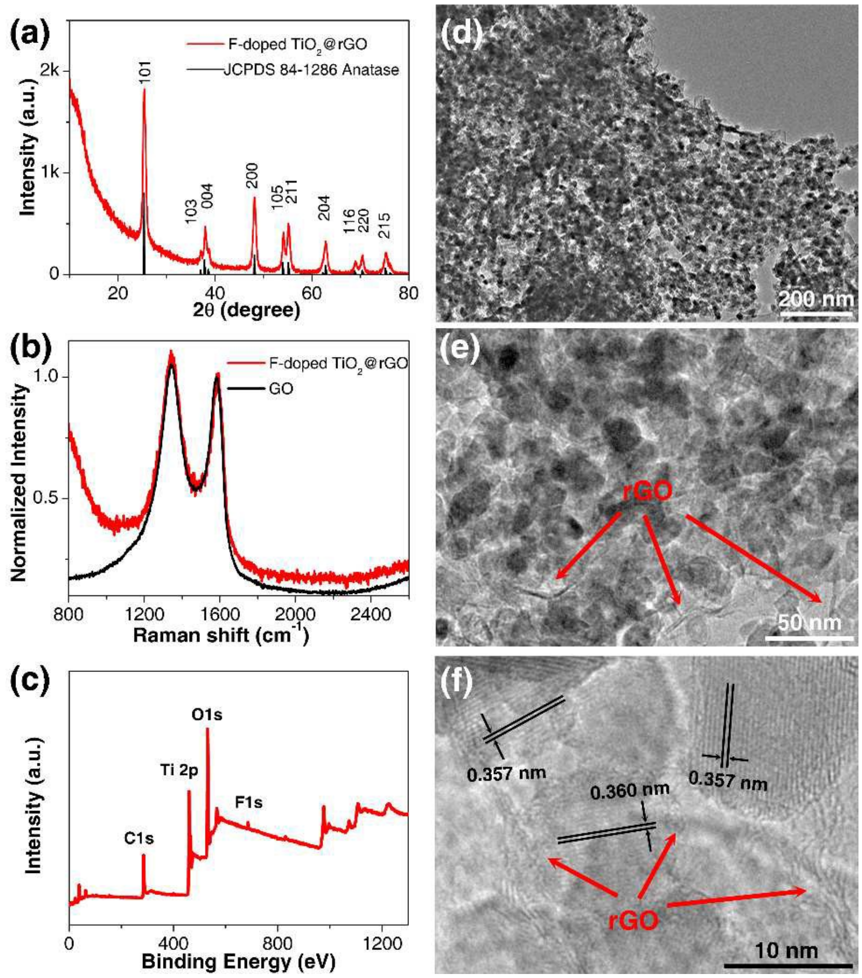

Figure 1 (a) X-ray diffraction (XRD) spectrum of the F-doped TiO_2@rGO heterojunction; (b) Raman spectra of the F-doped TiO_2@rGO heterojunction and GO; (c) XPS survey spectrum of the F-doped TiO_2@rGO heterojunction; (d) TEM, (e) Enlarged TEM and (f) HRTEM images of the F-doped TiO_2@rGO heterojunction.

3700DUV) using an integrating sphere and adopting $BaSO_4$ as a reference.

2.3. Photocatalytic measurement

The photodegradation of RhB was measured under UV-vis light irradiation (300 ≤ λ ≤ 2500 nm) at room temperature. The light source is a 300 W Xe-arc lamp (PLS-SXE300, Beijing). In a typical process, 30 mg of catalyst was firstly dispersed in 42 mL DI water, and then mixed with 18 mL of 100 mg/L RhB solution. Thus, the concentration of the final RhB solution is 30 mg/L. Before irradiation, the suspension was stirred in dark for 40 min to ensure the adsorption-desorption equilibrium. At a given time interval of 1 min, 2 mL solution was taken out and immediately centrifuged to remove the catalyst completely. In the durability test of the F-doped TiO_2@rGO heterojunction in the photodegradation of RhB under UV-vis light, three consecutive cycles were tested. After each cycle, the F-doped TiO_2@rGO heterojunction was filtered, washed thoroughly with water and annealed at 400 ^oC for 2 h. The concentration of the RhB solution was analyzed on a UV-vis spectrophotometer (UV-1800, Shimadzu). The pH value of the RhB solution was measured by a pH-meter (METTLER TOLEDO, PE20k) after completely removing the catalyst from solution (5 mL) by centrifugation.

3. Results and discussion

The preparation route of the F-doped TiO_2@rGO heterojunction is illustrated in Scheme 2. Generally, ice bath is adopted to ensure a slow hydrolyzation of $TiCl_4$ to form TiO_2 nanocrystal seeds with extremely small size on rGO sheets. The low temperature (50 ^oC) growth method could retard the rapid growth of TiO_2 nanocrystals in the solution. Thus, the further growth of TiO_2 on the seeds is expected to result in the dense and uniform growth of TiO_2 nanoparticles on rGO sheets. Moreover, the introduction of F-ion could enhance the photocatalytic activity of TiO_2 by improving the crystallinity of TiO_2.

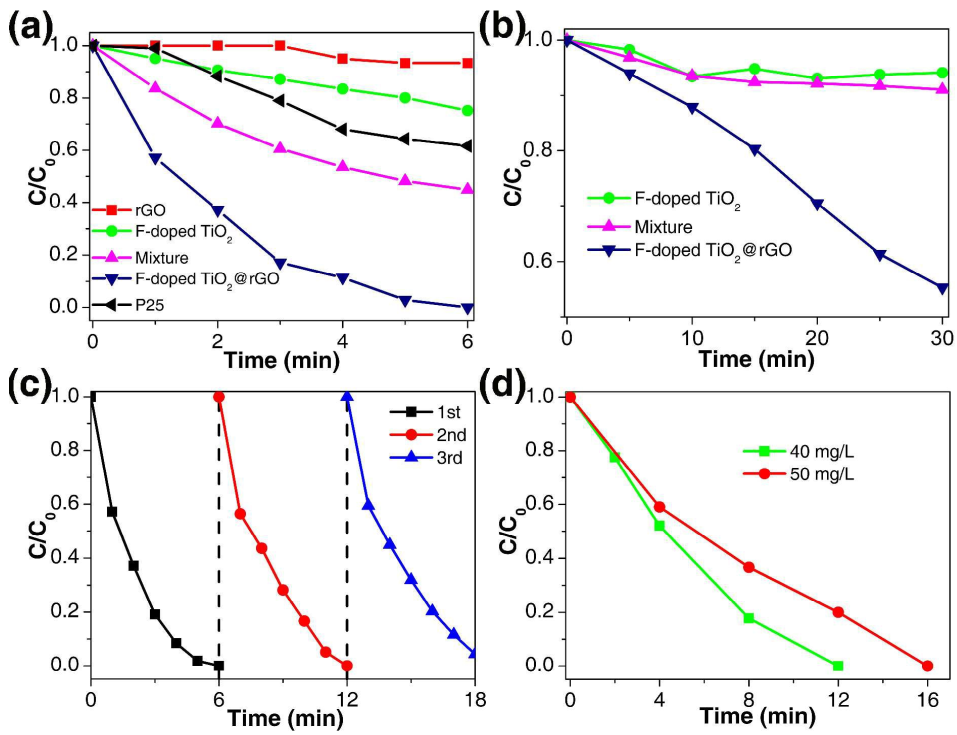

Figure 2 (a) The liquid-phase photodegradation performances of rGO, F-doped TiO_2, the physical mixture (F-doped TiO_2 and rGO) and F-doped TiO_2@rGO heterojunction towards RhB with time under UV-vis light irradiation ($300 \le \lambda \le 2500$ nm); (b) The liquid-phase photodegradation performance of the F-doped TiO_2, mixture, F-doped TiO_2@rGO towards RhB with time under visible light irradiation ($400 \le \lambda \le 2500$ nm); (c) Cycling photodegradation towards RhB; (d) The liquid-phase photodegradation performance of F-doped TiO_2@rGO heterojunction towards RhB (40 and 50 mg/L) with time under UV-vis light irradiation.

To investigate the crystal phases of the F-doped TiO_2@rGO heterojunction, X-ray diffraction (XRD) analysis was performed (Figure 1a). All the diffraction peaks are sharp, and can be indexed to anatase TiO_2 (JCPDS, 84-1286), suggesting a good crystallinity of TiO_2 nanoparticles. According to the Scherrer formula:

$$D = 0.89\lambda / \beta\cos(\theta) \qquad (1)$$

where D is average grain size, λ is the X-ray wavelength employed, θ is the diffraction angle, and β is the line broadening at half the maximum intensity after subtracting the instrumental broadening. The particle size of the decorated TiO_2 nanoparticles could be calculated by typical XRD peaks (Table S1). Taking the (101) diffraction peak as an example, the size of the TiO_2 nanoparticles in the F-doped TiO_2@rGO heterojunction is around 12 nm. From the Raman spectra (Figure 1b), the graphitized structures (D band (~1341 cm^{-1}) and G band (~ 1580 cm^{-1})) were observed in both the F-doped TiO_2@rGO heterojunction and GO. It is shown that there is no peak position shift of the F-doped TiO_2@rGO heterojunction compared with that of GO. Furthermore, the intensity ratio of D band over G band (I_D/I_G) increases from 1.05 to 1.09, indicating the reduction of GO with the hydrothermal treatment.[28, 49, 50] X-ray photoelectron spectroscopy (XPS) survey spectrum (Figure 1c) of the F-doped TiO_2@rGO shows that all the peaks of C, O, F and Ti can be observed, suggesting the presence of F, C and Ti species. The C 1s XPS signal shows that the three peaks at 284.6, 286.4, and 289.4 eV could be attributed to the C-C, C-O and C=O bonds in rGO-based composites (Figure S1a). Two peaks centered at 459.0 and 465.1 eV in the Ti 2p spectrum (Figure S1b) can be assigned to Ti 2p1/2 and Ti 2p3/2, respectively, which is in good agreement with the binding energy values of Ti^{4+} in pure anatase TiO_2, suggesting the formation of TiO_2 on the rGO sheets.[51]

Owing to the small particle size, the supported TiO_2 nanoparticles can be hardly observed in the scanning electron microscopy (SEM) image (Figure S2). Here, the TEM image of the F-doped TiO_2@rGO heterojunction confirms that the TiO_2 nanoparticles were densely and uniformly decorated on rGO sheets (Figure 1d). Compared with the previously reported TiO_2@rGO systems,[2, 17, 52] the decorated TiO_2 nanoparticles are much more dense and uniform in the present system. It is supposed that the formation of seeds in ice bath method greatly helps the *in-situ* growth of the TiO_2 nanoparticles on rGO sheets, favouring the photoinduced electron transfer from TiO_2 to rGO. Both the edge of rGO and the structure of the TiO_2 nanoparticles were shown in an enlarged TEM image (Figure 1e). RGO sheet behaves as a support for TiO_2 nanoparticles, and the TiO_2 nanoparticles are shaped due to the introduction of F-ion. The average size of the TiO_2 nanoparticles in F-doped TiO_2@rGO heterojunction is 13 nm (Figure S3), which is very consistent with the above calculated crystal size along (101) diffraction peak. All the observed

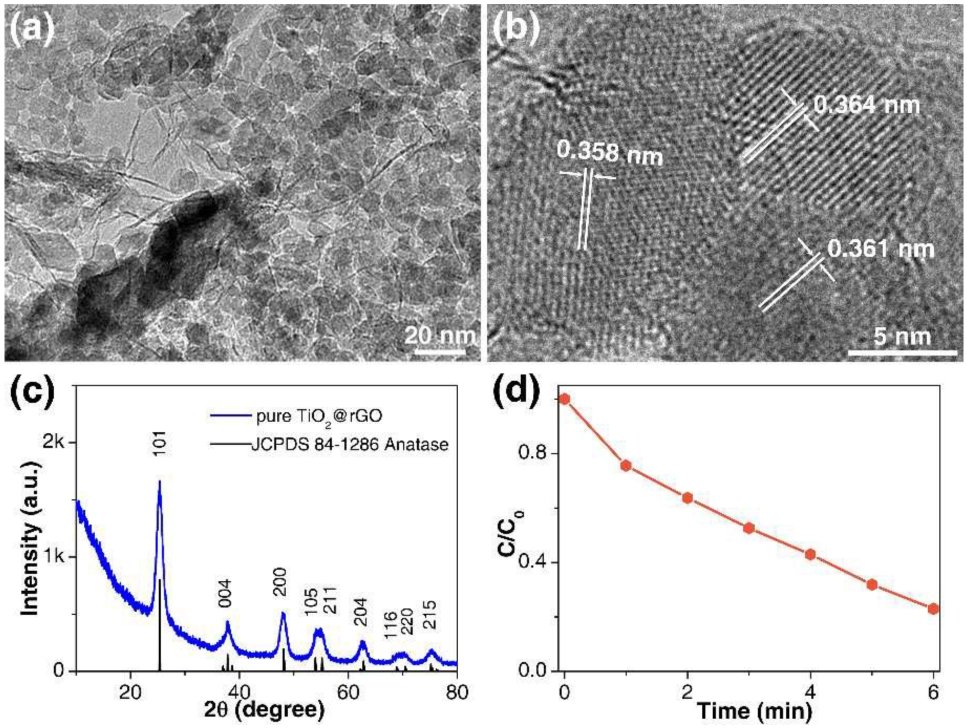

Figure 3 (a) The TEM image, (b) HRTEM image and (c) XRD pattern of the pure TiO_2@rGO heterojunction; (d) The liquid-phase photodegradation performance towards RhB.

lattice fringes of the shaped TiO_2 nanoparticles show a d-spacing of 0.357 to 0.360 nm (Figure 1f), which can be well assigned to the (101) lattice fringes of anatase TiO_2.

Figure 2a shows the photodegradation performance of the F-doped TiO_2@rGO heterojunction towards RhB with time under UV-vis light irradiation as a function of time. Here, C and C_0 represent the remaining concentration of dye solution with certain degradation time and after dark adsorption. And for comparison, the photodegradation performances of rGO, F-TiO_2, the mixture of F-TiO_2 and rGO, and P25 under the same condition are also shown. Before light irradiation, the RhB solutions with catalysts were maintained in dark for 40 min under stirring, this time period is proved to be long enough to reach the adsorption equilibrium as shown in Figure S4. And the remaining concentration of RhB was calibrated *via* the fitting curve (Figure S5). It is clearly shown that the F-doped TiO_2@rGO heterojunction possesses much better adsorption ability towards RhB compared with F-TiO_2, the mixture (F-TiO_2 and rGO), or P25 due to the present preparation route induced large surface area (Figure S6, S7 and Table S2), which can be attributed to the dense and uniform growth of TiO_2 on rGO and the little ratio of bare rGO between covered TiO_2 nanocrystals. The F-doped TiO_2@rGO heterojunction shows much better photocatalytic efficiency than F-doped TiO_2, suggesting the formation of heterojunction between F-doped TiO_2 and rGO. The photodegradation efficiency of F-doped TiO_2 increased from 25% to 100% with the formation of the heterojunction structure since it can greatly suppress the electron-hole recombination. Similarly, the performance of the F-doped TiO_2@rGO heterojunction is more efficient than P25 for the same reason. Moreover, the performance of the mixture of the same amount of F-doped TiO_2 and rGO was much lower than that of the F-doped TiO_2@rGO heterojunction. The remaining amount of RhB at 6 min was still 44.9% when the mixture was used as the photocatalyst. It should be noted that in the whole adsorption and degradation process, the pH value maintains at a constant value of around 5.8 (Figure S8), thus, the pH value has no effect on the RhB degradation rate during the whole process. Moreover, there is no obvious change in band gap of TiO_2 by the introduction of F-ion (Figure S9), confirming that the influence of light absorption by TiO_2 can be ignored. Thus, it is considered that the dense and uniform growth of TiO_2 nanocrystals on rGO greatly favours the adsorption of the majority of dyes on the surface of TiO_2. As a result, the final photodegradation efficiency of the F-doped TiO_2@rGO heterojunction is much higher than the simple mixture. This conclusion could be further supported by the much better photocatalytic performance of F-doped TiO_2@rGO heterojunction than those of F-TiO_2 and the mixture under visible light (Figure 2b). The photodegradation efficiencies of F-doped TiO_2@rGO and the mixture under visible light are 45% and 6% at 30 min, respectively. Considering that RhB solution is stable even under UV-vis light illumination (Figure S10), and holes in TiO_2 could not be generated, the efficient utilization of the photogenerated electrons in RhB molecules by the present F-doped TiO_2@rGO catalyst can be well confirmed. One should

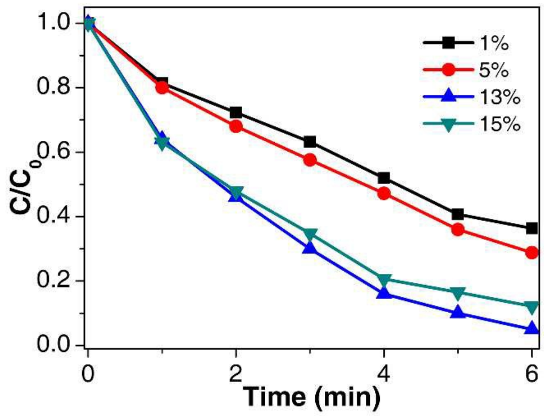

Figure 4. The liquid-phase photodegradation performances of F-doped TiO_2@rGO heterojunction with different weight ratios of rGO (1, 5, 13 and 15%) towards RhB under UV-vis light irradiation.

note that the photodegradation efficiency of F-doped TiO_2@rGO under visible light is only 7.2% at 6 min, which falls far behind that under UV-vis light illumination (100%), indicating that holes produced by the band-gap excitation of TiO_2 still plays a dominant role in the photodegradation process, while the dense and uniform growth of F-doped TiO_2 nanocrystals on rGO further enhances the photocatalytic efficiency by the efficient utilization of the photogenerated electrons in the target RhB molecules. Recyclability is another key factor for photocatalysts. Figure 2c shows 3 cycles of photodegradation of the F-doped TiO_2@rGO heterojunction towards RhB. It is proved that the good photocatalytic activity could be maintained perfectly after 3 cycles, implying the promising practical application potential of the F-doped TiO_2@rGO heterojunction. RhB solutions with high concentrations (40 and 50 mg/L) can also be photodegradated in 12 and 16 min with 30 mg F-doped TiO_2@rGO heterojunctions under UV-vis light irradiation (Figure 2d), which further confirms the practical application capability of the present F-doped TiO_2@rGO heterojunctions.

To confirm that the dense and uniform growth of TiO_2 nanoparticles on rGO can efficiently utilize the photogenerated electrons in the target RhB molecules, pure TiO_2@rGO heterojunction was also prepared to exclude the influence of F-ion on the crystallinity and morphology of TiO_2.[53, 54] The TEM and HRTEM images of the pure TiO_2@rGO heterojunction were shown in Figure 3a and 3b, respectively. From the Figure 3a, it can be found that TiO_2 nanoparticles also were densely and uniformly decorated on rGO sheets, suggesting the crucial role of the present preparation route to the dense growth of TiO_2 on rGO. And TiO_2 nanoparticles are spherical (compared with the shaped TiO_2 nanocrystals in Figure 1e). From the HRTEM image of the pure TiO_2@rGO heterojunction (Figure 3b), it can be found that the lattice fringes of TiO_2 show a d-spacing of 0.358 to 0.364 nm, which also can be well assigned to the (101) lattice fringes of TiO_2. It can be concluded that the introduction of F-ion could modulate the morphology of TiO_2. The corresponding average size of the spherical TiO_2 nanoparticles in the pure TiO_2@rGO heterojunction is 7 nm (Figure S11a), which agrees well with the surface and pore measurement results (Figure S11b and Table S2). All the diffraction peaks (Figure 3c) can also be indexed to anatase TiO_2 (JCPDS, 84-1286). However, the diffraction peaks are not as sharp as those of the F-doped TiO_2@rGO heterojunction, suggesting the crucial role of F-ion in improving the crystallinity of TiO_2 nanocrystals. The Figure 3d shows the photodegradation performance of the pure TiO_2@rGO heterojunction towards RhB under UV-vis light irradiation. When the photodegradation time is 6 min, the remaining amount of RhB is 19%, which is still more efficient than the mixture. It is further proved that the dense cover of TiO_2 nanocrystals on rGO sheets, no matter with or without the doping of F-ion, can help to efficiently utilize the photogenerated electrons in RhB and enhance the final photodegradation efficiency. However, with the help of F-ion, the photodegradation efficiency is even better considering the higher surface area of the pure TiO_2@rGO heterojunction (263 m^2/g, Table S2).

To further confirm the influence of the density and uniformity of TiO_2 on the photocatalytic performance, F-doped TiO_2@rGO heterojunctions with different weight ratios of rGO (1, 5, 13 and 15%) were prepared, and the surface areas of them are 53, 101, 203 and 182 m^2/g (Figure S12 and Table S2), respectively. It is found that these samples could degrade 64%, 29%, 95% and 88% of RhB within 6 min as shown in Figure 4, respectively. Although all these samples are much more efficient than the mixture (Figure 2a), the content of rGO can affect the photocatalytic activity of F-TiO_2@rGO remarkably. A lower content of rGO would not favour the growth of TiO_2 on rGO and there is free TiO_2 nanocrystals in the catalyst, thus, the photodegradation efficiency is low due to the inefficient separation of the electron-hole pairs. The excessive content of rGO would induce more RhB molecules adsorpted on rGO rather than on the surface of TiO_2, which would not benefit the efficient utilization of the photogenerated electrons in RhB molecules. Thus, it is considered that a proper content of rGO could realize the dense and uniform growth of TiO_2 on rGO sheets and to ensure the efficient separation of the electron-hole pairs and the sufficient adsorption of RhB molecules on TiO_2.

4. Conclusions

In conclusion, an ice bath hydrolyzation method is adopted to grow dense and uniform F-doped TiO_2 nanocrystals on rGO sheets. The as-prepared F-doped TiO_2@rGO heterojunction showed extremely high photocatalytic efficiency under UV-vis light irradiation compared with that of the commercial P25 and the mixture of F-TiO_2 and rGO. It is proved that the dense and uniform growth of TiO_2 nanocrystals on rGO greatly favors to utilize the photogenerated electrons in RhB. The pure TiO_2@rGO heterojunction is also much more efficient than the mixture of F-TiO_2 and rGO, proving that the ice bath hydrolyzation preparation route is crucial to ensure the dense and uniform growth of TiO_2 nanocrystals on rGO and improve the photodegradation efficiency of the final product. The present work presents a new idea on how to efficiently utilize the photogenerated electrons in the target organic pollutants.

Acknowledgements

We thank the financial supports from the National Natural Science Foundation of China (51372273), Xinjiang Program of Introducing High Level Talents, "Hundred Talents Program" of the Chinese Academy of Sciences.

Notes and references

‡ Linjuan Guo and Zheng Yang contribute equally to this work.

1. G. Modugno, G. Roati, F. Riboli, F. Ferlaino, R. J. Brecha and M. Inguscio, *Science*, 2002, **297**, 2240-2243.
2. H. Zhang, X. Lv, Y. Li, Y. Wang and J. Li, *ACS Nano*, 2010, **4**, 380-386.
3. A. Tanaka, K. Hashimoto and H. Kominami, *J. Am. Chem. Soc.*, 2012, **134**, 14526-14533.
4. C. Yang, Z. Wang, T. Lin, H. Yin, X. Lü, D. Wan, T. Xu, C. Zheng, J. Lin, F. Huang, X. Xie and M. Jiang, *J. Am. Chem. Soc.*, 2013, **135**, 17831-17838.
5. X. Fan, L. Zang, M. Zhang, H. Qiu, Z. Wang, J. Yin, H. Jia, S. Pan and C. Wang, *Chem. Mater.*, 2014, **26**, 3169-3174.
6. S. Han, L. Hu, N. Gao, A. A. Al-Ghamdi and X. Fang, *Adv. Funct. Mater.*, 2014, **24**, 3725-3733.
7. L. R. Grabstanowicz, S. Gao, T. Li, R. M. Rickard, T. Rajh, D.-J. Liu and T. Xu, *Inorg. Chem.*, 2013, **52**, 3884-3890.
8. X. Chen and S. S. Mao, *Chem. Rev.*, 2007, **107**, 2891-2959.
9. X. Chen, S. Shen, L. Guo and S. S. Mao, *Chem. Rev.*, 2010, **110**, 6503-6570.
10. M. Wang, J. Ioccozia, L. Sun, C. Lin and Z. Lin, *Energy Environ. Sci.*, 2014, **7**, 2182-2202.
11. M. R. Hoffmann, S. T. Martin, W. Choi and D. W. Bahnemann, *Chem. Rev.*, 1995, **95**, 69-96.
12. B. Zu, B. Lu, Z. Yang, Y. Guo, X. Dou and T. Xu, *J. Phys. Chem. C*, 2014, **118**, 14703-14710.
13. Z. Bian, T. Tachikawa, P. Zhang, M. Fujitsuka and T. Majima, *J. Am. Chem. Soc.*, 2014, **136**, 458-465.
14. Q. Wang, M. Zhang, C. Chen, W. Ma and J. Zhao, *Angew. Chem. Int. Ed.*, 2010, **49**, 7976-7979.
15. C. Chen, W. Ma and J. Zhao, *Chem. Soc. Rev.*, 2010, **39**, 4206-4219.
16. K. Woan, G. Pyrgiotakis and W. Sigmund, *Adv. Mater.*, 2009, **21**, 2233-2239.
17. Y. Zhang, Z.-R. Tang, X. Fu and Y.-J. Xu, *ACS Nano*, 2010, **4**, 7303-7314.
18. I. Y. Kim, J. M. Lee, T. W. Kim, H. N. Kim, H.-i. Kim, W. Choi and S.-J. Hwang, *Small*, 2012, **8**, 1038-1048.
19. W. Gao, M. Wang, C. Ran, X. Yao, H. Yang, J. Liu, D. He and J. Bai, *Nanoscale*, 2014, **6**, 5498-5508.
20. Z.-Y. Wu, C. Li, H.-W. Liang, J.-F. Chen and S.-H. Yu, *Angew. Chem. Int. Ed.*, 2013, **52**, 2925-2929.
21. H. Hu, Z. Zhao, W. Wan, Y. Gogotsi and J. Qiu, *Adv. Mater.*, 2013, **25**, 2219-2223.
22. H. Sun, Z. Xu and C. Gao, *Adv. Mater.* , 2013, **25**, 2554-2560.
23. W. Guo, C. Chen, M. Ye, M. Lv and C. Lin, *Nanoscale*, 2014, **6**, 3656-3663.
24. W. Guo, F. Zhang, C. Lin and Z. L. Wang, *Adv. Mater.*, 2012, **24**, 4761-4764.
25. G. Nagaraju, G. Ebeling, R. V. Goncalves, S. R. Teixeira, D. E. Weibel and J. Dupont, *J. Mol. Catal. A-Chem.*, 2013, **378**, 213-220.
26. K. Novoselov, A. Geim, S. Morozov, D. Jiang, M. Katsnelson, I. Grigorieva, S. Dubonos and A. Firsov, *Nature*, 2005, **438**, 201.
27. J. L. Gunjakar, I. Y. Kim, J. M. Lee, N.-S. Lee and S.-J. Hwang, *Energy Environ. Sci.*, 2013, **6**, 1008-1017.
28. Q. Xiang, J. Yu and M. Jaroniec, *J. Am. Chem. Soc.*, 2012, **134**, 6575-6578.
29. B. Qiu, M. Xing and J. Zhang, *J. Am. Chem. Soc.*, 2014, **136**, 5852-5855.
30. L. Guo, B. Zu, Z. Yang, H. Cao, X. Zheng and X. Dou, *Nanoscale*, 2014, **6**, 1467-1473.
31. B. Zu, Y. Guo and X. Dou, *Nanoscale*, 2013, **5**, 10693-10701.
32. W. Tu, Y. Zhou and Z. Zou, *Adv. Funct. Mater.*, 2013, **23**, 4996-5008.
33. A. S. Cherevan, P. Gebhardt, C. J. Shearer, M. Matsukawa, K. Domen and D. Eder, *Energy Environ. Sci.*, 2014, **7**, 791-796.
34. Y. H. Ng, S. Ikeda, M. Matsumura and R. Amal, *Energy Environ. Sci.*, 2012, **5**, 9307-9318.
35. I. V. Lightcap, T. H. Kosel and P. V. Kamat, *Nano Lett.*, 2010, **10**, 577-583.
36. G. Williams, B. Seger and P. V. Kamat, *ACS Nano*, 2008, **2**, 1487-1491.
37. P. Wang, J. Wang, T. Ming, X. Wang, H. Yu, J. Yu, Y. Wang and M. Lei, *ACS Appl. Mater. Inter.*, 2013, **5**, 2924-2929.
38. P. Zhu, N. A. Sreekumaran, S. Peng, S. Yang and R. Seeram, *ACS Appl. Mater. Inter.*, 2012, **4**, 581-585.
39. J. Sun, H. Zhang, L.-H. Guo and L. Zhao, *ACS Appl. Mater. Inter.*, 2013, **5**, 13035-13041.
40. J. Wang, P. Wang, Y. Cao, J. Chen, W. Li, Y. Shao, Y. Zheng and D. Li, *Appl. Catal. B: Environ.*, 2013, **136–137**, 94-102.
41. Y. Liang, H. Wang, H. S. Casalongue, Z. Chen and H. Dai, *Nano Res.*, 2010, **3**, 701-705.
42. C. Yang, Z. Wang, T. Lin, H. Yin, X. Lü, D. Wan, T. Xu, C. Zheng, J. Lin and F. Huang, *J. Am. Chem. Soc.*, 2013, **135**, 17831-17838.
43. D. Zhao, G. Sheng, C. Chen and X. Wang, *Appl. Catal. B: Environ.*, 2012, **111**, 303-308.
44. J. Zhang, Z. Xiong and X. Zhao, *J. Mater. Chem.*, 2011, **21**, 3634-3640.
45. Z. Xiong, L. Zhang, J. Ma and X. Zhao, *Chem. Commun. (Cambridge, U. K.)*, 2010, **46**, 6099-6101.
46. H. Cui, J. Zheng, P. Yang, Y. Zhu, Z. Wang and Z. Zhu, *ACS Appl. Mater. Inter.*, 2015, **7**, 11230-11238.
47. W. S. Hummers and R. E. Offeman, *J. Am. Chem. Soc.*, 1958, **80**, 1339-1339.
48. Y. Xu, L. Zhao, H. Bai, W. Hong, C. Li and G. Shi, *J. Am. Chem. Soc.*, 2009, **131**, 13490-13497.
49. S. Liu, J. Yu and M. Jaroniec, *J. Am. Chem. Soc.*, 2010, **132**, 11914-11916.
50. L. Xiao, D. Wu, S. Han, Y. Huang, S. Li, M. He, F. Zhang and X. Feng, *ACS Appl. Mater. Inter.*, 2013, **5**, 3764-3769.
51. S. K. Joung, T. Amemiya, M. Murabayashi and K. Itoh, *Chem. Eur. J.*, 2006, **12**, 5526-5534.
52. T. N. Lambert, C. A. Chavez, B. Hernandez-Sanchez, P. Lu, N. S. Bell, A. Ambrosini, T. Friedman, T. J. Boyle, D. R. Wheeler and D. L. Huber, *J. Phys. Chem. C*, 2009, **113**, 19812-19823.
53. J. C. Yu, J. Yu, W. Ho, Z. Jiang and L. Zhang, *Chem. Mater.*, 2002, **14**, 3808-3816.
54. G. Wu, J. Wang, D. F. Thomas and A. Chen, *Langmuir*, 2008, **24**, 3503-3509.

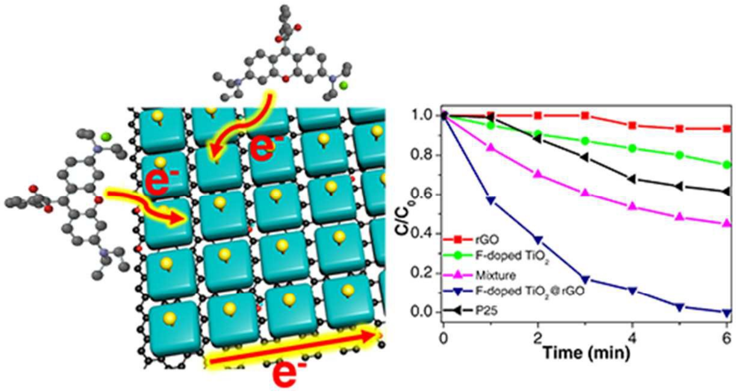

The F-doped TiO_2 densely and uniformly decorated on rGO sheet could adsorb more RhB on TiO_2 and efficiently utilize the photogenerated electrons of excited RhB to improve the photodegradation efficiency.